Biomimetic neurovascularized engineered muscle tissue for craniofacial volumetric muscle loss

Sijia Ding1, Shengjie Li1, Zhuojie Shen1, Yuhua Chen1, Xia Wang1,
Jianxiang He1†, Huiming Wang1, 2†, Mengfei Yu1†

1Key Laboratory of Oral Biomedical Research of Zhejiang Province, Stomatology Hospital, School of Stomatology, Zhejiang University School of Medicine, Zhejiang Provincial Clinical Research Center for Oral Diseases, Cancer Center of Zhejiang University, Hangzhou 310006, China
2The First Affiliated Hospital of Zhejiang University School of Medicine, School of Stomatology, and Key Laboratory of Oral Biomedical Research of Zhejiang Province, Hangzhou, Zhejiang, 310003, China

* These authors contributed equally: Sijia Ding, Shengjie Li and Zhuojie Shen.
† Correspondence: Mengfei Yu (yumengfei@zju.edu.cn); Huiming Wang (whmwhm@zju.edu.cn); Jianxiang He (hejianxiang@zju.edu.cn)

Abstract

Craniofacial muscles represent essential components of the skeletal muscle system, contributing to critical physiological processes. Severe trauma can result in craniofacial volumetric muscle loss (VML), hindering the muscle regenerative process and leading to muscular facial deformities and functional impairment, as well as social isolation and psychological depression. Conventional therapies, involving muscle flap transposition or autologous tissue grafting, only achieve morphological repair but are ineffective in restoring muscle function, often causing complications of donor-area injury and sensory deficit. In this study, we successfully constructed a biomimetic engineered muscle tissue that integrates myofiber alignment, effective innervation, and blood perfusion, which can promote multiple tissue regeneration of the masseter area in vivo, making functional regeneration achievable. Based on light-controlled micropatterning technology, we generated mature muscle fibers with oriented alignment and established a neuromuscular co-culture system for in vitro neuromuscular junction (NMJ) reconstruction. Additionally, we designed and fabricated a vascular network structure to promote the vascularization of tissue, with hydrogel serving as the vehicle for assembling the composite engineered tissue. This technology enables the capability to customize the shape and dimension of the constructed entity to address diverse muscle defects, enabling the goal of personalized repair. In summary, this study provides a promising novel strategy for tissue regeneration that breaks through the current challenges in the treatment of craniofacial VML.

Keywords: Tissue engineering, biomimetics, masticatory muscles, biomaterials, regenerative medicine

Introduction

Skeletal muscle, the most abundant tissue in the human body, accounting for approximately 40% of the total mass [1], plays critical roles in locomotion and metabolism [2]. It can be further classified into three main groups based on the location and function: trunk muscles, head and neck muscles, and limb muscle groups. The head muscles, differ from other muscle groups due to their distinct origins and development, as well as the underlying regulatory cascades [3, 4]. While not primarily participating in locomotion, the head skeletal muscles, serve in food uptake, respiration, and control over the cranial opening and vision, which are all crucial for survival [5]. In addition, the masticatory muscle, which serves as an important part of the head muscle [6], is capable of generating occlusal pressure with great force while allowing extremely high precision movements [7]. Such specialized physiological and functional features ensure the pressure balance of the muscles and dentition in the maxillofacial region, which is essential for maintaining symmetrical facial morphology and normal occlusal relations [8].

Severe trauma can lead to volumetric muscle loss (VML), which hinders the muscle regenerative process and can lead to persistent atrophy [9-11]. For this extensive muscle defect, while current clinical treatments through muscle flap transposition or autologous tissue grafting can provide cosmetic improvement, there come with complications such as donor-area morbidity and sensory deficits [12]. These methods can only achieve morphologic repair but are ineffective when it comes to improving muscle structure and function [13]. Furthermore, the lack of satellite cells in the masticatory muscle region may contribute to poor regenerative ability in response to acute damage [14, 15], making craniofacial VML treatment more challenging. Therefore, developing a novel tissue engineering strategy that can achieve both morphological and functional muscle repair holds great promise.

In the natural state, masticatory muscle owns distinct structural characteristics and unique physiological functions [7]. It consists of numerous ordered muscle fibers that can contract in a controlled and directed manner to generate force, which is the foundation for performing contractive functions [16, 17]. In addition, routine chewing and articulating functions necessitate muscle with great occlusal strength and accurate occlusal location [18]. Thus, modulation of the alignment of myoblasts is critical for tissue engineering to achieve functional recovery of masticatory muscle. Furthermore, neuralization and vascularization are inextricably connected to physiological muscle function and long-term survival. Effective innervation is essential for muscle signaling [19]. Denervation of skeletal muscle can lead to atrophy within three weeks, which can progress to irreversible fibrosis after two years without reinnervation [20]. Additionally, the abundant blood supply is essential for sustaining the muscle's high metabolic activity and delivering vital nutrients and oxygen [21]. Although current engineering strategies can facilitate muscle regeneration, their capacity for repairing surrounding nerves and vessels is markedly limited.

This study aims to bridge the research gap in tissue engineering for repairing craniofacial VML. Through the application of various advanced technologies, we were able to create mature muscle fibers that were aligned in a specific direction and to establish a neuromuscular co-culture system that allows for in vitro neuromuscular junction (NMJ) reconstruction. In addition, the mature vascular network structure was further constructed, and hydrogel was employed as the vehicle to assemble the three-dimensional neurovascularized engineered muscle tissue. This construct precisely mimics the structure and characteristics of natural muscle, and can promote multiple

tissue regeneration of masseter area in vivo (Fig. 1), which may provide a novel therapeutic strategy for achieving neurovascularized muscle regeneration in the field of craniofacial muscle tissue engineering.

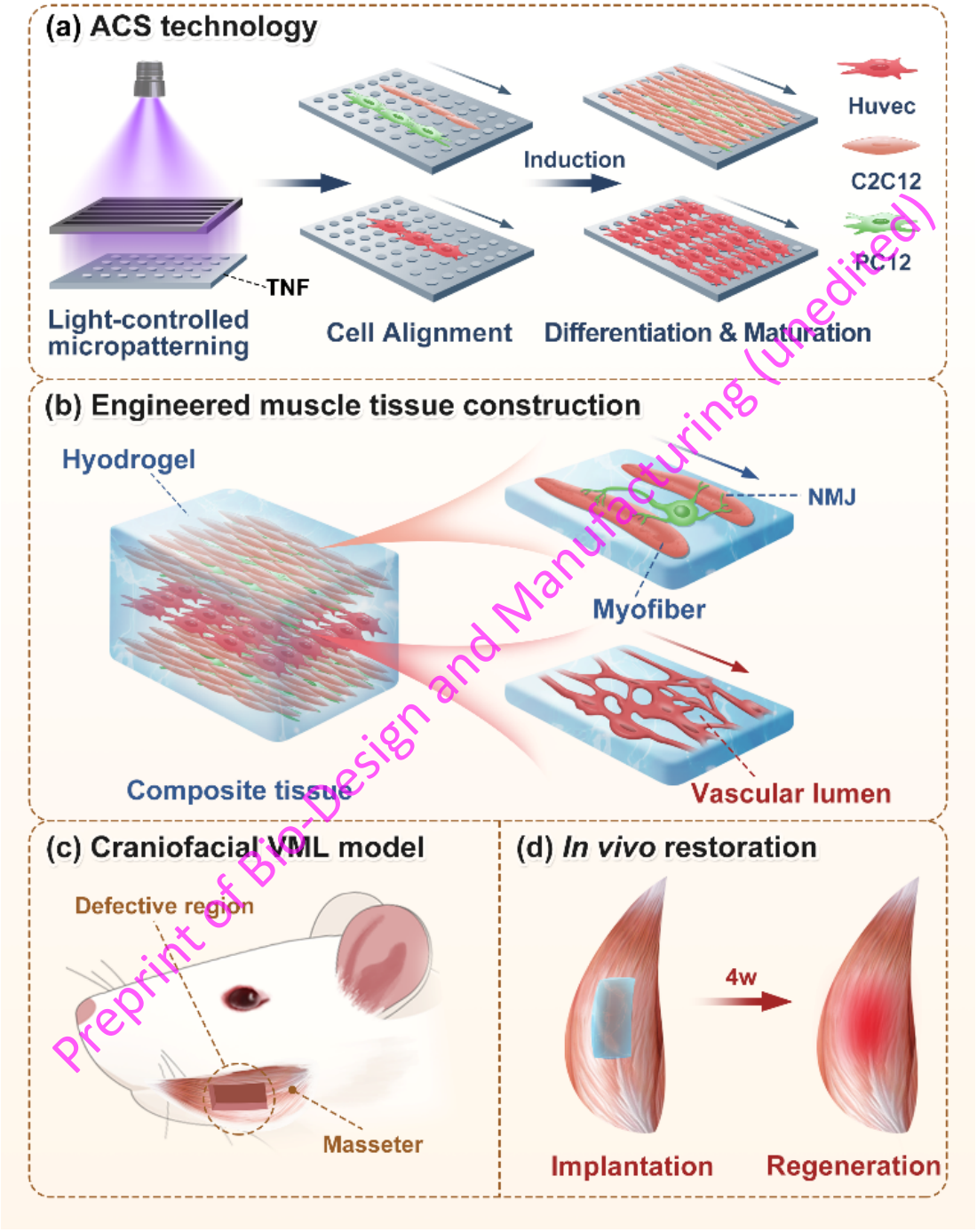

Fig.1 Schematic diagram for the fabrication of biomimetic neurovascularized engineered muscle tissue for craniofacial volumetric muscle loss.

Results

1. Light-controlled micropatterning induces cell alignment

To construct aligned cell sheets, a parallel-patterned mask was placed above the TiO2 nanodots

film (TNF), followed by UV light exposure for micro-patterning. C2C12 myoblasts were then seeded on the patterned TNF (Fig. 2a), employing methods consistent with prior research within our research group [22]. Fig. 2b displays cells cultured for 2 days, subjected to immunofluorescence staining for filamentous actin (F-actin) to assess cell orientation. It can be observed that cells in the Align group arrange along a defined direction, whereas the Non-Align group exhibits disordered and random arrangements. Quantitative analysis of cellular orientation further confirmed the feasibility of this approach for regulating cell alignment (Fig. 2c). Using electrical stimulation to induce cell contraction, the unidirectional contraction ability of the myoblasts in two groups was compared. Results revealed that material carrying aligned cells could bend along one direction, whereas the Non-Align group showed less bending (Fig. 2d). Quantitative results also confirmed this discrepancy, suggesting the potential capacity of alignment in enhancing cell functionality (Fig. 2e).

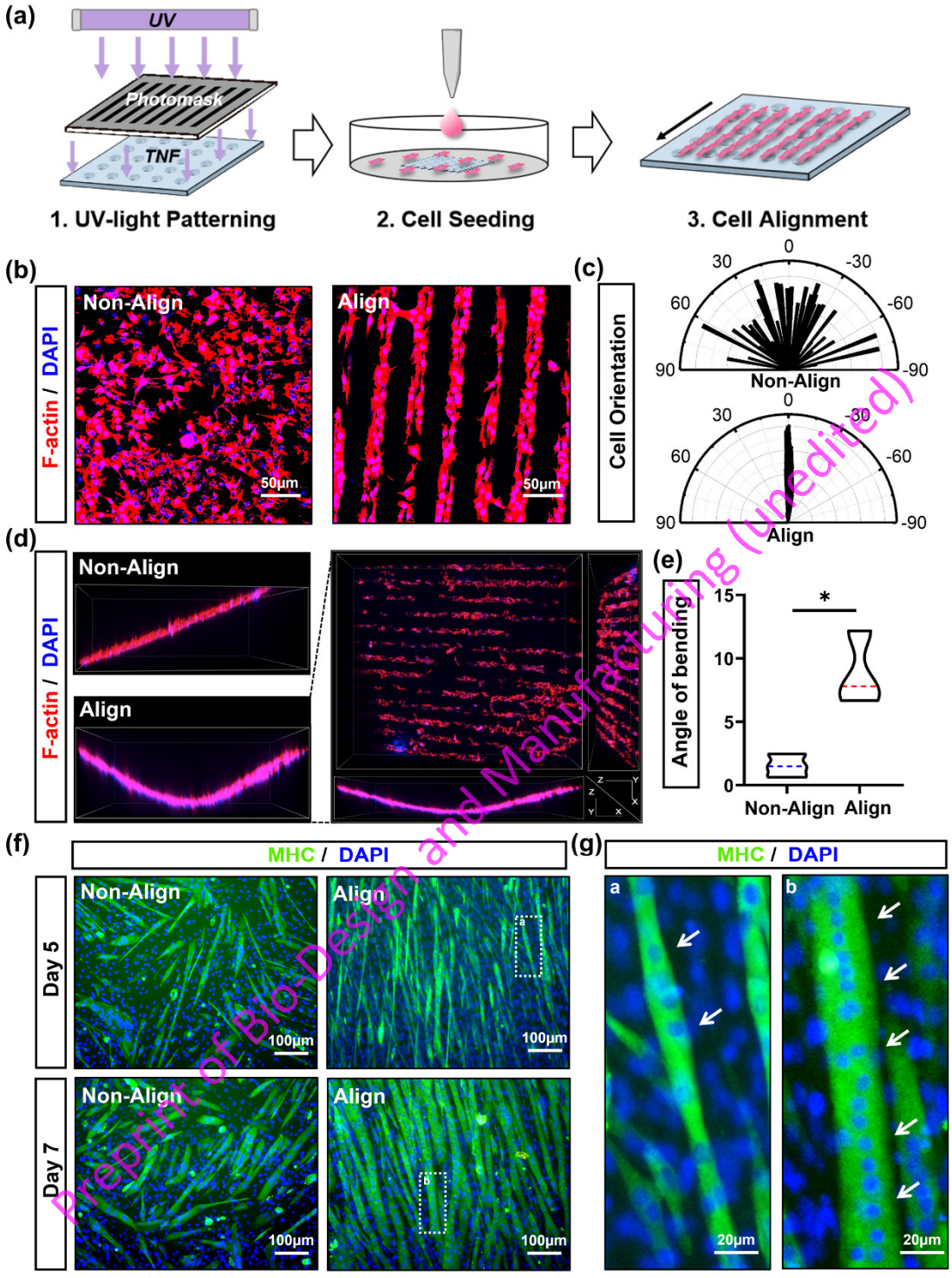

Fig. 2 Light-controlled micropatterning induces cell alignment and promotes myogenesis. a Schematic illustration of the procedure of the light-controlled micropatterning technology to induce cell alignment. b Immunofluorescence for F-actin (red)/DAPI (blue) of C2C12s cultured in unpatterned and patterned TNF as the Non-Align and Align group at 24h. c Quantitative analysis of cell orientation among two groups (n=20 per group). d Confocal images of z-stack showed the bending of PVDF carrying C2C12s under electrical stimulation. e Quantification of bending angle (n=5 per group). f Immunofluorescence for myogenic marker MHC (green)/ DAPI (blue) of C2C12s for 5 and 7 days of myogenic differentiation. g Comparison of MHC+ multinuclear myotubes after

5 and 7 days of differentiation. All data are represented as mean ± SD. The p-values by t-test are indicated. *p<0.05.

2. Cell alignment promotes myogenic differentiation

C2C12 cells were cultured separately on micro-patterned and untreated TNF surfaces, designated as the Align and Non-Align groups, respectively. Following induction with myogenic differentiation medium for 5 and 7 days, immunofluorescent staining for Myosin Heavy Chain (MHC) was performed to label differentiated and mature muscle fibers. The results indicated that muscle fibers formed in the Align group exhibited superior area and diameter compared to the Non-Align group (Fig. 2f). Additionally, after 7 days of induction, more fused nuclei were observed in the Align group compared to the 5 day induction, suggesting a more mature structural development (Fig. 2g). This result is further supported by the quantitative analysis of myofiber length and nuclei fusion in each group (Fig. S1). Based on those findings, we indicated that myoblasts alignment can promote myogenic differentiation, with more extended periods of aligned culture yielding more favorable myogenic outcomes.

3. Neuro-muscle cell co-culture system

To further accelerate the neural innervation of muscle tissue, we added PC12 neuronal cells into the C2C12 cell culture in a two-dimensional system. We selected six different co-culture ratios and compared the myogenic differentiation outcomes among groups. The immunofluorescent results demonstrated a notable increase in myofiber formation when the C2C12: PC12s quantity is at the ratio of 100:1 (Fig. 3a). Quantitative results also confirmed that it attained more myofiber area and greater width (Fig. 3b and 3c). Besides, it has been noticed that when the ratio exceeded 50:1, the myofiber area was reduced, suggesting excessive non-myogenic cells would instead hinder myogenesis. Therefore, in pursuit of optimizing myogenic differentiation conditions, subsequent experiments involving neuromuscular cell co-culture will choose the ratio of 100:1.

4. Construction of aligned neurovascularized engineered tissue

Using the above-mentioned light-controlled cell alignment technique, we constructed two structures: the aligned neuromuscular layer and the vascular network layer. Neuromuscular co-cultured cells were added in predetermined proportions and arranged in alignment. After 7 days of differentiation, both two structures exhibited mature morphology. Specifically, C2C12s fused and differentiated into multi-nucleated myotubes, while PC12s distributed around the myotubes, showing the differentiated morphology of axon extension (Fig. 3d). In addition, the location of the NMJs was marked by the acetylcholine receptors (ACHR) specific staining, further confirming the mutual binding site of the two cell types (Fig. 3e).

HUVECs were used to construct the aligned capillary-like network, and red fluorescent protein (RFP) was used for cell labeling and tracking. Under microscopy, cells were observed to be arranged in a specific direction (Fig. 3f). Additionally, staining of the F-actin cytoskeleton revealed its fused reticular morphology, confirming the mature appearance of the structure (Fig. 3g). Subsequently, both structures were transferred and stacked using photocurable hydrogel to assemble the aligned "sandwich" structure with the neuromuscular layer on the upper and lower layers and the vascular layer in the middle (Fig. 3h).

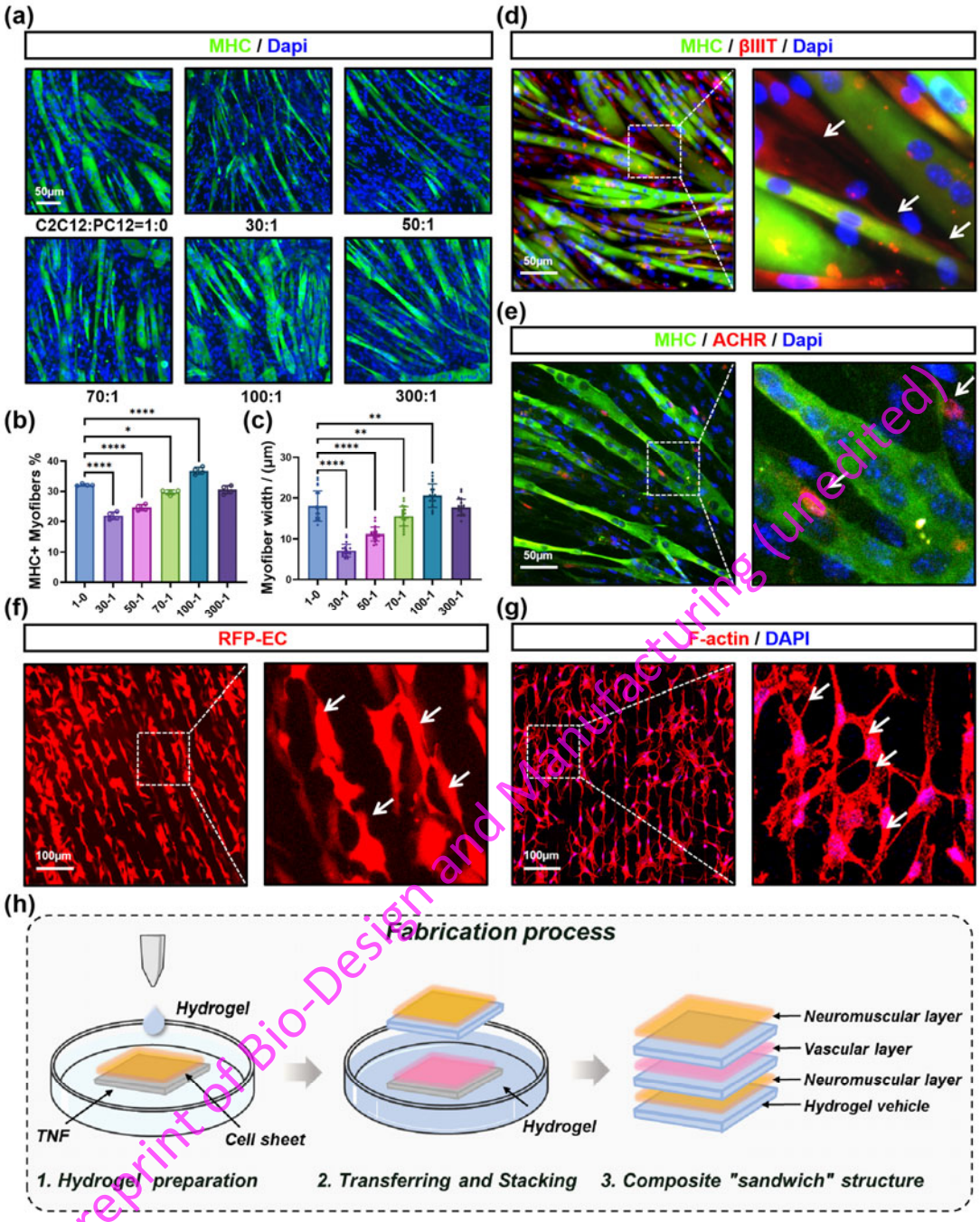

Fig. 3 Construction of aligned neurovascularized composite “sandwich” structure. a Immunofluorescence for MHC (green)/DAPI (blue) of C2C12s and PC12s in different ratios during co-culture for 7 days in a two-dimensional culture system. b Quantitative analysis of MHC+ myofibers areas (%) among groups (n=4 per group). c Quantitative analysis of MHC+ myofibers widths (μm) (n=20 per group). d Double-immunofluorescence for MHC (green)/ βIIIT (red)/DAPI (blue) of C2C12s and PC12s in co-culture at ratio of 100:1. The differentiated morphology of neuronal axon extension (white arrows). e Double-immunofluorescence for MHC (green)/ ACHR (red)/DAPI (blue). The location of AChR clustering and NMJ (white arrows). f Real-time fluorescence imaging of aligned capillary-like network formed by RFP-labeled HUVECs. g Immunofluorescence for F-actin (red)/ DAPI (blue). The capillary-like reticular structure (white

arrows). h Diagram of the fabrication process of composite “sandwich” structure. All data are represented as mean ± SD. The p-values by one-way ANOVA followed by Tukey’s test are indicated. ns $p>0.05$, **$p<0.01$, ****$p<0.0001$.

5. Craniofacial VML model construction and engineered tissue implantation

We established a craniofacial VML model in nude mice by surgically removing approximately 40%-50% of the masseter muscle volume (Fig. 4a). This critical muscle defect cannot be spontaneously healed and can result in persistent muscle atrophy and dysfunction. Then, we selected appropriately sized constructs based on the defective size and morphology and implanted them along the direction. Additionally, the Non-Align group, Sham group, and Defect group were set as the control group. Fig. 4b showed the entire surgical procedure.

6. Histological analysis

After 4 weeks of restoration, the histological structure of the masseter in each group was observed by hematoxylin-eosin (H&E) and Masson trichromic staining (MTS), respectively. The Defect group exhibited obvious muscle atrophy and fiber degeneration, whereas the implant group all showed an increase in muscle weight (Fig. 4e). The Non-Align group showed partial muscle repair, but the fiber distribution was disordered (Fig. 4c). Notably, in the Align group, the regenerated muscle fibers were regular in shape, basically arranged along the direction (Fig S2), and exhibited reduced fibrous scar area, suggesting better muscle repair ability (Fig. 4d and 4f). In addition, the hydrogel implanted in the defect site could integrate with the original muscle and showed substantial degradation (Fig. S3), verifying the effective biocompatibility and degradation ability of the constructed tissue.

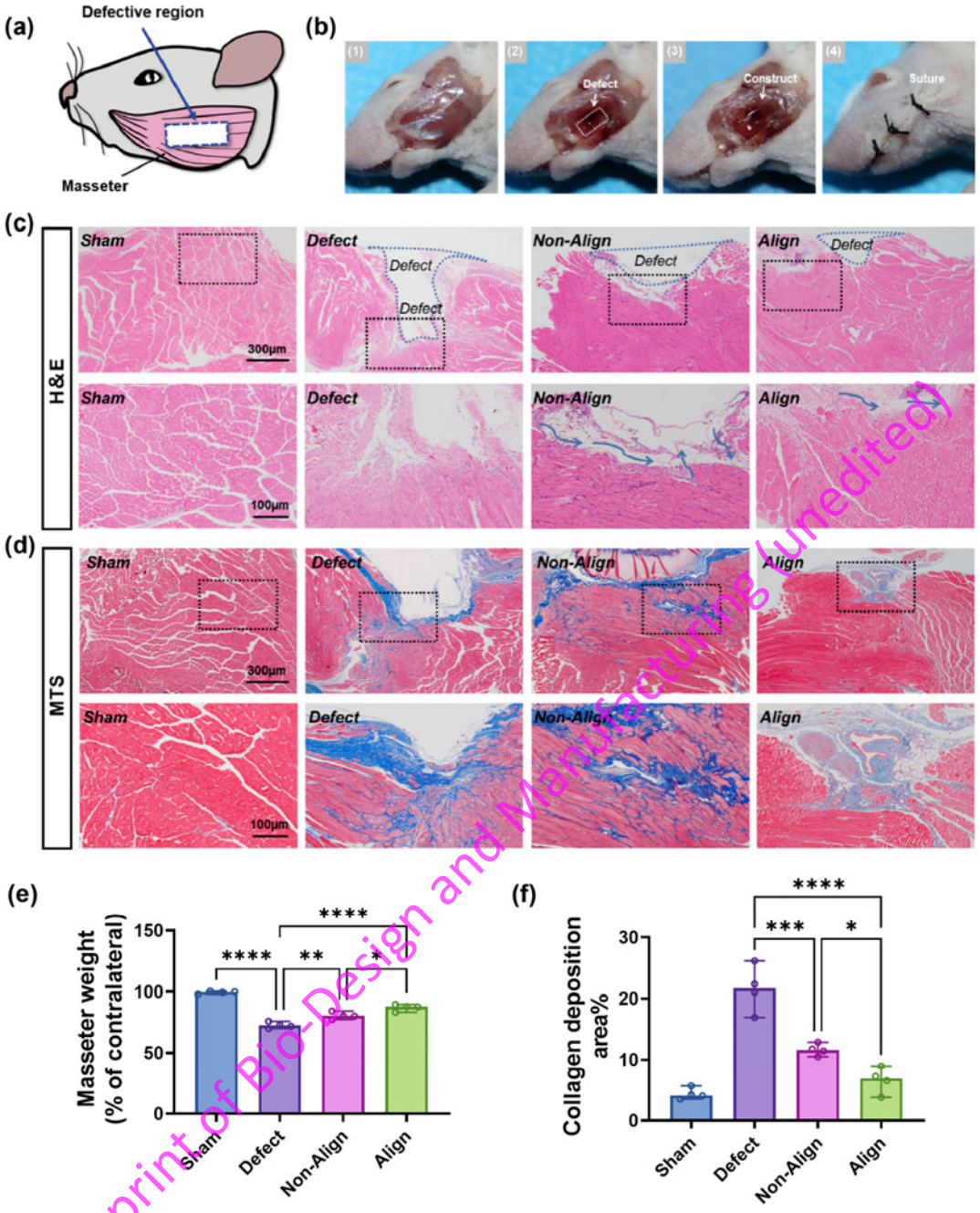

Fig. 4 Composite neurovascularized engineered muscle tissue implantation promoted the restoration of masseter. a Schematic illustration of the defective region of the masseter muscle in mice. b Surgical procedure containing the construction of the masseter defect and the implantation of the engineered tissue. c, d Hematoxylin and eosin (H&E) and masson's trichome staining (MTS) of the surgical areas after 4 weeks repairment. (n=4 per group) (Black dashed box: enlarged area, Blue dashed box: defective area, Arrow: direction of the newborn muscle fibers, Blue stained area: fibrous scar tissue). e Quantification of masseter weight (% of contralateral normal muscle) at 4 weeks after implantation. f Quantification of the collagen deposition area (%) using MTS results (n=4 per group). All data are represented as mean ± SD. The p-values by one-way ANOVA followed by Tukey's test are indicated. *p<0.05, **p<0.01, ***p<0.001, ****p<0.0001.

7. Evaluation of in vivo composite tissue regeneration

To clarify the construct's impact on the composite tissue of muscle, nerve, and vessel, we analyzed the specific markers of MHC, beta-III tubulin (βIIIT), ACHR, and platelet endothelial cell adhesion molecule-1 (CD31), in each group's repaired tissue. The evaluation criteria for muscle tissue structure based on histological staining results primarily involve: muscle tissue morphology, size of muscle fibers, arrangement of muscle fibers, and distribution of fibrous tissue. Notably, the Align group exhibited a significant increase in MHC+ myofiber area, and the morphology closely resembled that of the Sham group (Fig. 5a and 5b). Specifically, the newly formed muscle fibers in the Align group showed distinct boundaries, and their size and arrangement more closely resembled those of the Sham group. The areas of the neuronal differentiation marker βIIIT and the NMJ-related marker ACHR were increased in the Align group, both suggesting better neural innervation (Fig. 5c, 5d and Fig S4). Furthermore, a rise in CD31+ vascular lumen in Align group was observed, suggesting the ability of engineered tissue to promote new blood vessel formation in vivo (Fig. 5e and 5f). Antibodies from distinct species were used to label the nerves and vessels of both host and engineered tissues, revealing areas of mutual integration and co-localization (Fig. 5g and 5i). The results of double-staining immunofluorescence confirmed the engineered tissue's ability to integrate with the host tissue, with more integrating sites in the Align group compared to the Non-Align (Fig. 5h and 5j).

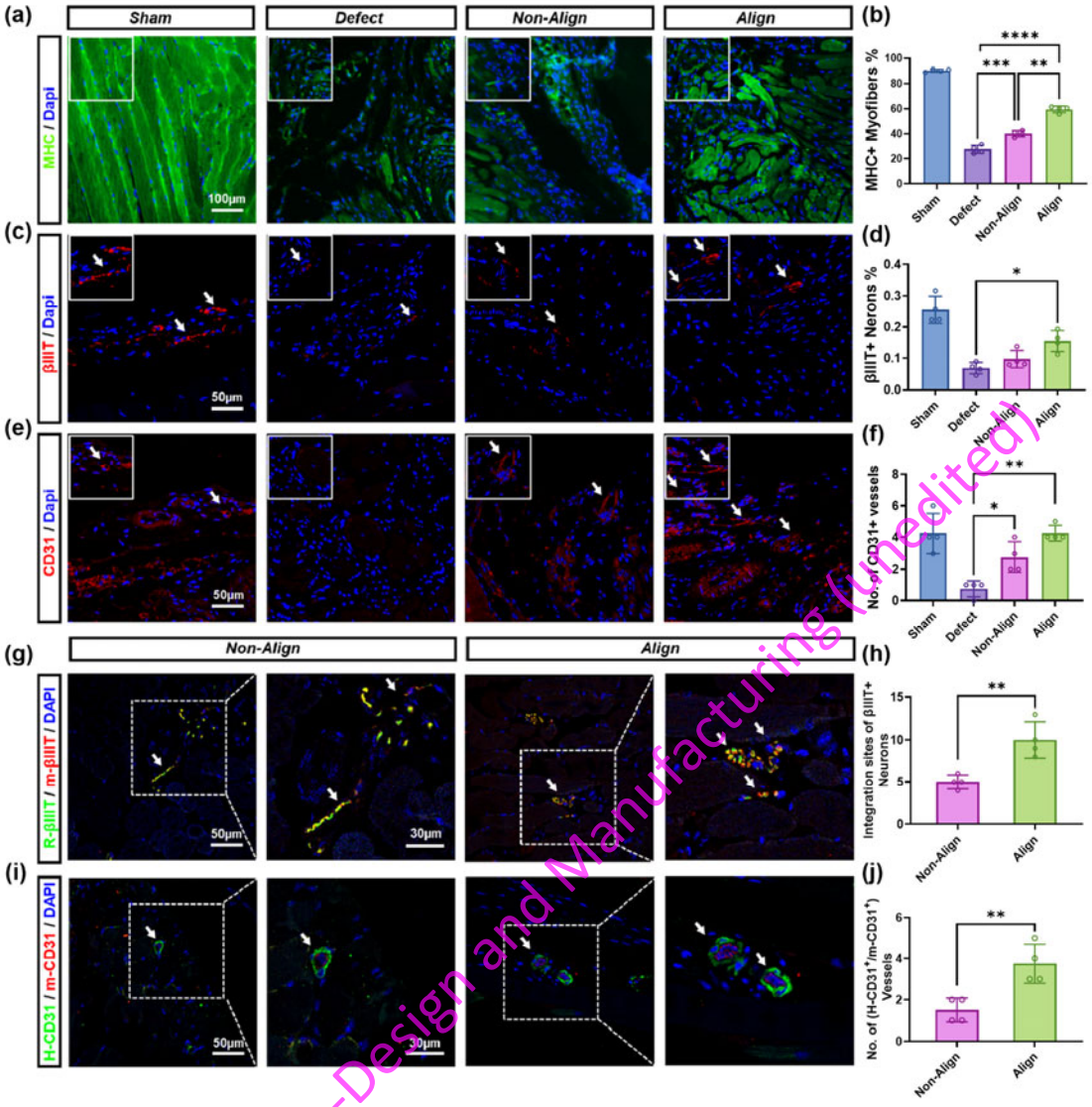

Fig. 5 Composite tissue regeneration of the masseter region after 4 weeks of restoration. a Immunofluorescence for myogenic marker MHC (green)/ DAPI (blue) of surgical area of masseter muscle at 4 weeks restoration. (White squares: magnified image of target area). b Quantification of the areas of MHC+ myofibers (%). c Immunofluorescence for neural marker βIIIT (red)/ DAPI (blue) of surgical area. (White arrows: βIIIT + neurons). d Quantification of the areas of βIIIT + neurons (%). e Immunofluorescence for vascular marker CD31 (red)/ DAPI (blue) of surgical area. (White arrows: CD31+ vascular lumens). f Quantification of the numbers of CD31+ vascular lumens. g Immunofluorescence for βIIIT of rat species (R-βIIIT) labeled the host (green)/ mice species (m-βIIIT) labeled the implanted (red)/ DAPI (blue). h Quantification of the integration site of R-βIIIT+/ m-βIIIT+ neurons. i Immunofluorescence for CD31 of human species (H-CD31) (green)/ mice species (m-CD31) (red)/DAPI (blue). j Quantification of the number of H-CD31+/ m-CD31+ vessels (n=4 per group). All data are represented as mean ± SD. The p-values by one-way ANOVA followed by Tukey's test or t-test are indicated. *p<0.05, **p<0.01, ***p<0.001, ****p<0.0001.

8. Functional evaluation

To further compare the recovery of masseter function among the groups, we measured the food intake per unit time and the body weight changes of mice among 4 weeks of restoration. The results showed a marked decrease in both body weight and food intake in the defect group. Although the Non-Aligned group exhibited an upward trend, there was no significant difference compared to the defect group. Notably, the Align group demonstrated considerably higher food intake and body weight, confirming its better functional recovery compared to the other groups (Fig. S5a and S5b).

Discussion

In the musculature of the craniofacial region, the masseter muscle constitutes a crucial component, playing a pivotal role in maintaining functions related to mastication and phonation. However, when it sustains substantial defects due to trauma or surgical procedures, it can lead to craniofacial VML, which causes severe muscular functional impairment and facial deformities [23-25]. Currently, in the field of muscle tissue engineering, there have been numerous studies focusing on the reconstruction of large-scale skeletal muscle defects [26-28]. However, limited attention has been given to the musculature of the craniofacial region. Recent reconstruction strategies revolve around the development of biocompatible scaffolds with varying properties to emulate the physiological characteristics of natural tissues[29, 30]. These approaches include the construction of ordered scaffolds to facilitate the directional alignment of muscle fibers [31], enhancing the strength and stiffness of scaffolds to match natural tissues [32], and simulating muscle contraction activities [33], among other methods, to explore more optimal treatment approaches. By simulating the structural features, these methods can encourage muscle ingrowth by inducing microenvironments or as a cell delivery vehicle [34]. However, they exhibit limited capacity for the repair of surrounding nerves and blood vessels. Furthermore, it has been proposed that functional recovery deficits are primarily due to the limited rate and extent of vascularization and neural innervation of the implanted engineered tissue, leading to the atrophy of the engineered muscle before functional integration with surrounding host tissues occurs [35].

Denervation has long been disregarded in the VML pathophysiology. VML can disrupt motor neurons and NMJs, altering the innervation of skeletal muscles, resulting in acute denervation of muscle fibers within the remaining muscle tissue and ongoing deterioration within six months [36]. In addition, investigations on spinal cord and peripheral nerve injury have demonstrated that innervation is intimately tied to muscle contractility and the excitation-contraction coupling [37, 38], which can be critical for the restoration of muscle strength. Among these, the NMJs may serve as a critical site in signal transmission and the re-establishment of innervation inside muscle tissue. Serving as a specialized interface between motor neurons and their innervated skeletal muscle fibers, the NMJs convert action potentials from motor neurons into effective muscle contractions [39]. Through the response to action potentials of motor neurons and subsequent acetylcholine release, muscle fibers undergo membrane depolarization, voltage-gated calcium channels open, and intracellular calcium levels increase, thereby initiating activation of the contractile apparatus [40]. These studies have provided further evidence for our in vitro reconstruction of NMJs and the realization of innervation in muscle tissue.

According to our research findings, the addition of a small proportion of PC12s can effectively accelerate myogenic differentiation and the formation of NMJs through neuromuscular co-culture. Co-cultured cells can promote intercellular signal transmission and induce the

activation of intracellular signal transduction pathways through direct cellular contact [41]. Moreover, neural cells are capable of producing and releasing a variety of growth factors and neurotrophic factors, including nerve growth factor (NGF), glial cell line-derived neurotrophic factor (GDNF) and neuropeptide [42], which can act on myoblasts to promote their growth and differentiation. The addition of PC12s may also alter the microenvironment in the co-culture system, thereby creating conditions more conducive for myogenic differentiation. While the addition of a small number of PC12s has been proven to accelerate the myogenic process, the introduction of a large number of non-myogenic cells can hinder the fusion and differentiation of myoblasts [43], thus making it crucial to determine the appropriate cell co-culture ratio.

In this study, we employed an available and easily operable approach to control the directional alignment of muscle cells, resulting in the construction of matured oriented muscle fibers, thereby enhancing unidirectional muscle contraction force. Simultaneously, we established a neural-muscle in vitro co-culture system to elucidate the interaction between nerve and muscle cells, confirming the feasibility of establishing NMJs in vitro. Additionally, we implemented a pre-vascularization strategy to enhance the post-transplantation survival prospects of engineered tissue and mitigate tissue hypoxia[44]. Utilizing hydrogels as the assembly matrix not only effectively retained extracellular matrix cues but also circumvented a range of issues associated with implanting scaffolds, including biocompatibility and degradation concerns. Moreover, the presence or absence of scar tissue is a crucial factor in the recovery of muscle function. Scar tissue, lacking the elasticity and contractility of muscle tissues, can lead to impaired function when accumulated excessively, affecting muscle flexibility and strength. Our treatment approach, by enhancing muscle regeneration efficiency and reducing scar tissue formation, has facilitated more functional tissue regeneration and showed satisfying results, which may offers a promising treatment option for functional regeneration of craniofacial muscles.

While this research holds promise for developing a novel therapeutic approach in reconstructive surgery, its biosafety and long-term efficacy require further evaluation in practical applications. Future work will focus on enhancing technical aspects and advancing clinical translation. Moreover, we will delve into the interactions among muscles, nerves, and blood vessels, seeking to uncover their specific mechanisms of action.

Materials and Methods

1. TNF preparation and UV light-controlled cell alignment.

Titanium dioxide nanodot films (TNFs) were prepared on the surface of quartz substrates using a phase separation-induced self-assembly approach as previously reported [45]. First, a precursor sol consisting of a mixture of tetrabutyl titanate (TBOT, Sinopharm Chemical Reagents), acetylacetone (AcAc, Lingfeng Chemical Reagents), and polyvinylpyrrolidone (PvP, Sinopharm Chemical Reagents) was prepared and spin-coated onto the surface of the quartz substrate (10 × 10 × 1 mm3). Then, the substrates were heat-treated at 500°C for 1 h. After autoclaving and drying, the TNFs were stored in a dark room for subsequent cell culture.

The UV micropatterning of TNF was performed with a designed photomask as previously reported [22]. A UV light source (254 nm, 300 μW/cm2) was used to pass through the photomask to form the micropatterns of parallel lines with width spacing of 30 μm. After that, immediately moving to the well plate with tweezers, and cells were added to the substrate to align along the micropattern.

2. Cell culture.

The C2C12 myoblasts, PC12 neural cells, and HUVEC endothelial cells were purchased from the American Type Culture Collection (ATCC, USA). C2C12s and PC12s were cultured in Dulbecco's modified Eagle's medium (DMEM/high glucose) with 10% fetal bovine serum (FBS) according to the instructions. HUVECs were cultured in vascular cells basal medium supplemented with Endothelial Cell Growth Kit-VEGF (ECGM, ATCC).

All the cells were incubated at 37 °C in an atmosphere of 5% CO2, media replaced fresh every 2 days, and cells were harvested at 80% confluence. C2C12s (1*105) were seeded into each TNF and cultured in the DMEM with 10% FBS. To construct the differentiated myotubes, the growth medium was changed to myogenic differentiation medium (DMEM/high glucose containing 2% horse serum) after 24h to further induce differentiation for 7 days.

3. In vitro contractional testing.

The conductive material polyvinylidene fluoride (PVDF) was cut into 1cm x 1cm pieces, and attached to the cells cultured on the TNF. After 1 min of exposure to UV-light, the cell sheet was transferred to the PVDF surface. Using the electrical stimulator (CUY21EDIT II, BEX) to induce cell contraction, with two electrodes connected to each end of the material. Following electrical stimulation with the same parameters for each group, the bending degree of the PVDF was promptly measured.

4. Co-culture system.

The PC12 and C2C12 cells were counted, respectively, and the two cell suspensions were pre-mixed according to the set different ratios (1:0, 30:1, 50:1,70:1, 100:1, 300:1) then added into 24-well plates for co-culture. The growth medium (DMEM/high glucose containing 10% FBS) was selected on the first day and replaced with differentiation medium (DMEM/high glucose containing 2% horse serum, nerve growth factor (NGF), 50ng/ml) on the second day, and cells were collected for evaluation after 7 days of co-culture.

5. Immunofluorescent staining.

First, samples were fixed with 4% paraformaldehyde, permeabilized with 0.05% Triton X 100/PBS, blocked with 2% BSA solution, and then incubated with the configured primary antibody solution at 4°C overnight. Primary antibody: MYH(b-5) (sc376157, Santa Cruz, Europe); βIIIT (ab18207, Abcam, USA); AChR (ab41174, Abcam, USA). Next day after rewarming and washed off, incubated with the configured secondary antibody for 1h. After washing off, the nuclei were stained with 4′,6-diamidino-2-phenylindole (DAPI). Secondary antibodies: AlexaFluor 488-labeled IgG antibody (Dawen, China); AlexaFluor 594-labeled IgG antibody (Dawen, China). F-actin cytoskeleton staining was performed using Rhodamine-phalloidin (Cytoskeleton, USA). Fluorescence was detected using the inverted fluorescence microscope (ThermoFisher, USA) and the confocal laser scanning microscope (Nikon, Japan).

6. Preparation of GelMA hydrogel.

The GelMA prepolymer solution was prepared at 10% concentration as previously reported [22]. The GelMA solution, which was melted after heating, was added to the fused cells on the TNF and then UV-illuminated from the bottom of the plate. After 1 min of illumination, the solidified GelMA was removed from the TNF with blade, and cell sheet adhering to its surface. It is possible to further transfer and stack different cell sheets using the same strategy to prepare three-dimensional multilayer structures.

7. Construction of composite tissue.

The PC12 and C2C12 cells are mixed and co-cultured on the TNFs surface in the above ratio, and after 7 days of differentiation, the cells are fused to form the neuromuscular layer. In addition, HUVECs can form the capillary-like network layer after 3 days of differentiation using the same strategy. The engineering tissue completed the stacking and assembly of different tissue layers in vitro, using GelMA to make the layers stick to each other, forming a whole construct by assembling in the sequential order of the neuromuscular layer in the upper and lower layers and the capillary-like network layer in the middle layer.

8. Craniofacial VML nude mice model.

According to the authorized method, masseter defects were created in immunodeficient male nude mice aged 8 weeks. Firstly, anesthetize the mice with sodium pentobarbital, the surface skin was cut to expose the masseter area, and about 40-50% of the muscle volume was removed with the scalpel. Following hemostasis and cleaning, a suitable construct was selected based on the defect site and transplanted along the direction of the muscle fibers. GelMA is applied around the edge of the construct for adhesion and fixation after photocuring, ensuring that the engineered tissue is well fixed in the target area. A total of four groups were set up: 1. Sham group (sham operation only), 2. Defect group (no treatment) 3. Non-Align group (implantation of non-aligned construction) 4. Align group (implantation of aligned construction), the recovery of mice in each group was detected after 4 weeks of implantation.

9. Histological analysis.

At 4 weeks after surgery, the masseter muscles of the mice were isolated, collected and fixed in 4% paraformaldehyde (Sigma, Aldrich). Then, the tissues were dehydrated, embedded in paraffin, and sliced into 8-um-thick slices. The paraffin slices were stained with H&E (Sigma, Aldrich) and MTS (Sigma, Aldrich). Histological features were determined using microscopy, and the fibrosis area was determined and quantified using the ImageJ program. Regarding tissue localization of the section, the target tissue area is located by referring to the site of the excised muscle, observing the remaining hydrogel and the boundary between the hydrogel and the muscle tissue.

10. Functional evaluation

After surgery completion and again after 4 weeks of restoration, mice in each group were weighed using a scale to record their body weights and analyze differences before and after. Subsequently, following a 12-hour fasting period, mice were provided with standard food in feeders, and the food intake within a fixed time frame (10 minutes) was recorded for each group of mice.

11. Statistical analysis.

All data were presented as the mean ± standard deviations (SD). For statistical analyses, the one-way analysis of variance (ANOVA) or the t-test was employed with the programs of GraphPad Prism and SPSS Statistics. A p-value of <0.05 was considered statistically significant.

Acknowledgements: This work was financially supported by National Natural Science Foundation of China (82122014, 82071085, 82020108011, 82301031), Zhejiang Provincial Natural Science Foundation of China (LR21H140001), the National Key Research and Development Program of China (2018YFA0703000), Medical Technology and Education of Zhejiang Province of China (2018KY501), Foundation of Zhejiang University (2022QZJH55).

Author contributions: S.D., S.L., Z.S. contributed equally to this work. S.D., S.L.,: Conception and design, collection and assembly of data, data analysis and interpretation, manuscript writing; Z.S., X.W.: Materials production and data analysis; Y.C.: Manuscript revision and literature collection; J.H., H.W., M.Y.: Conception and design, financial support, administrative support, manuscript revision, final approval of manuscript. All authors have read and approved the final manuscript.

Competing interests: The authors declare that they have no competing interests.

Ethical approval: This project was approved by Zhejiang University Animal Care and Use Committee. The approval code number is ZJU20230192. All institutional and national guidelines for the care and use of laboratory animals were followed.

Data and materials availability: All data generated or analyzed during this study are available in the main text or the supplementary materials.

References

1. Janssen I., Heymsfield S. B., Wang Z. M. and Ross R. (2000) Skeletal muscle mass and distribution in 468 men and women aged 18-88 yr. Journal of Applied Physiology (Bethesda, Md. : 1985) 89(1):81-88. https//doi.org/10.1152/jappl.2000.89.1.81

2. Wang Z., Yang J., Sun X., Sun X., Yang G. and Shi X. e. (2023) Exosome-mediated regulatory mechanisms in skeletal muscle: A narrative review. Journal of Zhejiang University. Science. B 24(1) https://doi.org/10.1631/jzus.B2200243

3. Bailey P., Holowacz T. and Lassar A. B. (2001) The origin of skeletal muscle stem cells in the embryo and the adult. Current Opinion In Cell Biology 13(6):679-689. https//doi.org/10.1016/s0955-0674(00)00271-4

4. Mootoosamy R. C. and Dietrich S. (2002) Distinct regulatory cascades for head and trunk myogenesis. Development (Cambridge, England) 129(3):573-583. https//doi.org/10.1242/dev.129.3.573

5. Schubert F. R., Singh A. J., Afoyalan O., Kioussi C. and Dietrich S. (2019) To roll the eyes and snap a bite - function, development and evolution of craniofacial muscles. Seminars In Cell & Developmental Biology 91:31-44. https://doi.org/10.1016/j.semcdb.2017.12.013

6. Wachtler F. and Jacob M. (1986) Origin and development of the cranial skeletal muscles. Bibliotheca Anatomica (29):24-46.

7. Isola G., Anastasi G. P., Matarese G., Williams R. C., Cutroneo G., Bracco P. and Piancino M. G. (2018) Functional and molecular outcomes of the human masticatory muscles. Oral Diseases 24(8):1428-1441. https://doi.org/10.1111/odi.12806

8. Shirakawa T., Miyawaki A., Kawamoto T. and Kokabu S. (2021) Natural compounds attenuate denervation-induced skeletal muscle atrophy. International Journal of Molecular Sciences 22(15)

https://doi.org/10.3390/ijms22158310
9. Garg K., Ward C. L., Hurtgen B. J., Wilken J. M., Stinner D. J., Wenke J. C., Owens J. G. and Corona B. T. (2015) Volumetric muscle loss: Persistent functional deficits beyond frank loss of tissue. Journal of Orthopaedic Research : Official Publication of the Orthopaedic Research Society 33(1):40-46. https://doi.org/10.1002/jor.22730
10. L'Heureux N. and Letourneur D. (2015) Clinical translation of tissue-engineered constructs for severe leg injuries. Annals of Translational Medicine 3(10):134. https://doi.org/10.3978/j.issn.2305-5839.2015.05.03
11. Aguilar C. A., Greising S. M., Watts A., Goldman S. M., Peragallo C., Zook C., Larouche J. and Corona B. T. (2018) Multiscale analysis of a regenerative therapy for treatment of volumetric muscle loss injury. Cell Death Discovery 4:33. https://doi.org/10.1038/s41420-018-0027-8
12. Gholobova D., Terrie L., Gerard M., Declercq H. and Thorrez L. (2020) Vascularization of tissue-engineered skeletal muscle constructs. Biomaterials 235:119708. https://doi.org/10.1016/j.biomaterials.2019.119708
13. Daigeler A., Drücke D., Tatar K., Homann H.-H., Goertz O., Tilkorn D., Lehnhardt M. and Steinau H.-U. (2009) The pedicled gastrocnemius muscle flap: A review of 218 cases. Plastic and Reconstructive Surgery 123(1):250-257. https://doi.org/10.1097/PRS.0b013e3181904e2e
14. Ono Y., Boldrin L., Knopp P., Morgan J. E. and Zammit P. S. (2010) Muscle satellite cells are a functionally heterogeneous population in both somite-derived and branchiomeric muscles. Developmental Biology 337(1):29-41. https://doi.org/10.1016/j.ydbio.2009.10.005
15. Pavlath G. K., Thaloor D., Rando T. A., Cheong M., English A. W. and Zheng B. (1998) Heterogeneity among muscle precursor cells in adult skeletal muscles with differing regenerative capacities. Developmental Dynamics : an Official Publication of the American Association of Anatomists 212(4):495-508. https//doi.org/10.1002/(SICI)1097-0177(199808)212:4<495::AID-AJA3>3.0.CO;2-C
16. Furusawa K., Kawahana Y. and Miyashita R. (2023) Construction of engineered muscle tissue consisting of myotube bundles in a collagen gel matrix. Gels (Basel, Switzerland) 9(2). https://doi.org/10.3390/gels9020141
17. Shadrach J. L. and Wagers A. J. (2011) Stem cells for skeletal muscle repair. Philosophical Transactions of the Royal Society of London. Series B, Biological Sciences 366(1575):2297-2306. https://doi.org/10.1098/rstb.2011.0027
18. McComas A. J. (1998) Oro-facial muscles: Internal structure, function and ageing. Gerodontology 15(1). https//doi.org/ 10.1111/j.1741-2358.1998.00003.x
19. Bongers K. S., Fox D. K., Ebert S. M., Kunkel S. D., Dyle M. C., Bullard S. A., Dierdorff J. M. and Adams C. M. (2013) Skeletal muscle denervation causes skeletal muscle atrophy through a pathway that involves both gadd45a and hdac4. American Journal of Physiology. Endocrinology and Metabolism 305(7):E907-E915. https://doi.org/10.1152/ajpendo.00380.2013
20. Adidharma W., Khouri A. N., Lee J. C., Vanderboll K., Kung T. A., Cederna P. S. and Kemp S. W. P. (2022) Sensory nerve regeneration and reinnervation in muscle following peripheral nerve injury. Muscle & Nerve 66(4):384-396. https://doi.org/10.1002/mus.27661
21. Adams R. H. and Alitalo K. (2007) Molecular regulation of angiogenesis and lymphangiogenesis. Nature Reviews. Molecular Cell Biology 8(6):464-478.
22. Liu C., Zhou Y., Sun M., Li Q., Dong L., Ma L., Cheng K., Weng W., Yu M. and Wang H. (2017) Light-induced cell alignment and harvest for anisotropic cell sheet technology. ACS Applied

Materials & Interfaces 9(42):36513-36524. https://doi.org/10.1021/acsami.7b07202
23. Lew T. A., Walker J. A., Wenke J. C., Blackbourne L. H. and Hale R. G. (2010) Characterization of craniomaxillofacial battle injuries sustained by united states service members in the current conflicts of iraq and afghanistan. Journal of Oral and Maxillofacial Surgery : Official Journal of the American Association of Oral and Maxillofacial Surgeons 68(1):3-7. https://doi.org/10.1016/j.joms.2009.06.006
24. Gassner R., Tuli T., Hächl O., Rudisch A. and Ulmer H. (2003) Cranio-maxillofacial trauma: A 10 year review of 9,543 cases with 21,067 injuries. Journal of Cranio-maxillo-facial Surgery : Official Publication of the European Association For Cranio-Maxillo-Facial Surgery 31(1):51-61. https://doi.org/10.1016/j.joms.2009.06.006
25. De Sousa A. (2008) Psychological issues in oral and maxillofacial reconstructive surgery. The British Journal of Oral & Maxillofacial Surgery 46(8):661-664. https://doi.org/10.1016/j.bjoms.2008.07.192
26. Jana S., Cooper A. and Zhang M. (2013) Chitosan scaffolds with unidirectional microtubular pores for large skeletal myotube generation. Advanced Healthcare Materials 2(4):557-561. https://doi.org/10.1002/adhm.201200177
27. Chen S., Nakamoto T., Kawazoe N. and Chen G. (2015) Engineering multi-layered skeletal muscle tissue by using 3d microgrooved collagen scaffolds. Biomaterials 73:23-31. https://doi.org/10.1016/j.biomaterials.2015.09.010
28. Kroehne V., Heschel I., Schügner F., Lasrich D., Bartsch J. W. and Jockusch H. (2008) Use of a novel collagen matrix with oriented pore structure for muscle cell differentiation in cell culture and in grafts. Journal of Cellular and Molecular Medicine 12(5A):1640-1648. https://doi.org/10.1111/j.1582-4934.2008.00238.x
29. Zhang B., Xue Q., Hu H.-Y., Yu M.-F., Gao L., Luo Y.-C., Li Y., Li J.-T., Ma L., Yao Y.-F. and Yang H.-Y. (2019) Integrated 3d bioprinting-based geometry-control strategy for fabricating corneal substitutes. Journal of Zhejiang University. Science. B 20(12):945-959. https://doi.org/10.1631/jzus.B1900190
30. Aazmi A., Guo Z., Yu H., Lv W., Ji Z., Yang H. and Ma L. (2024) Enhanced mixing efficiency for a novel 3d tesla micromixer for newtonian and non-newtonian fluids. Journal of Zhejiang University-SCIENCE A 24(12):1065-1078. https://doi.org/10.1631/jzus.A2300589
31. Guan J., Fujimoto K. L. and Wagner W. R. (2008) Elastase-sensitive elastomeric scaffolds with variable anisotropy for soft tissue engineering. Pharmaceutical Research 25(10):2400-2412. https://doi.org/10.1007/s11095-008-9628-x
32. Christensen K. W., Turner J., Coughenour K., Maghdouri-White Y., Bulysheva A. A., Sergeant O., Rariden M., Randazzo A., Sheean A. J., Christ G. J. and Francis M. P. (2022) Assembled cell-decorated collagen (ac-dc) fiber bioprinted implants with musculoskeletal tissue properties promote functional recovery in volumetric muscle loss. Advanced Healthcare Materials 11(3):e2101357. https://doi.org/10.1002/adhm.202101357
33. Zhao L., Zhang X., Luo Q., Hou C., Xu J. and Liu J. (2020) Engineering nonmechanical protein-based hydrogels with highly mechanical properties: Comparison with natural muscles. Biomacromolecules 21(10):4212-4219. https://doi.org/10.1021/acs.biomac.0c01002
34. Wolf M. T., Dearth C. L., Sonnenberg S. B., Loboa E. G. and Badylak S. F. (2015) Naturally derived and synthetic scaffolds for skeletal muscle reconstruction. Advanced Drug Delivery Reviews 84:208-221. https://doi.org/10.1016/j.addr.2014.08.011

35. Rousseau E., Raman R., Tamir T., Bu A., Srinivasan S., Lynch N., Langer R., White F. M. and Cima M. J. (2023) Actuated tissue engineered muscle grafts restore functional mobility after volumetric muscle loss. Biomaterials 302:122317. https://doi.org/10.1016/j.biomaterials.2023.122317
36. Sorensen J. R., Hoffman D. B., Corona B. T. and Greising S. M. (2021) Secondary denervation is a chronic pathophysiologic sequela of volumetric muscle loss. Journal of Applied Physiology (Bethesda, Md. : 1985) 130(5):1614-1625. https://doi.org/10.1152/japplphysiol.00049.2021
37. Sulaiman W. and Gordon T. (2013) Neurobiology of peripheral nerve injury, regeneration, and functional recovery: From bench top research to bedside application. Ochsner Journal 13(1):100-108.
38. Kern H., Boncompagni S., Rossini K., Mayr W., Fanò G., Zanin M. E., Podhorska-Okolow M., Protasi F. and Carraro U. (2004) Long-term denervation in humans causes degeneration of both contractile and excitation-contraction coupling apparatus, which is reversible by functional electrical stimulation (fes): A role for myofiber regeneration? Journal of Neuropathology and Experimental Neurology 63(9):919-931. https//doi.org/ 10.1093/jnen/63.9.919
39. Lin C.-Y., Yoshida M., Li L.-T., Ikenaka A., Oshima S., Nakagawa K., Sakurai H., Matsui E., Nakahata T. and Saito M. K. (2019) Ipsc-derived functional human neuromuscular junctions model the pathophysiology of neuromuscular diseases. JCI Insight 4(18) https://doi.org/10.1172/jci.insight.124299
40. Kuo I. Y. and Ehrlich B. E. (2015) Signaling in muscle contraction. Cold Spring Harbor Perspectives In Biology 7(2):a006023. https://doi.org/10.1101/cshperspect.a006023
41. Kuppusamy P., Kim D., Soundharrajan I., Hwang I. and Choi K. C. (2020) Adipose and muscle cell co-culture system: A novel in vitro tool to mimic the in vivo cellular environment. Biology 10(1) https://doi.org/10.3390/biology10010006
42. Narayanan N., Lengemann P., Kim K. H., Kuang L., Sobreira T., Hedrick V., Aryal U. K., Kuang S. and Deng M. (2021) Harnessing nerve-muscle cell interactions for biomaterials-based skeletal muscle regeneration. Journal of Biomedical Materials Research. Part A 109(3):289-299. https://doi.org/10.1002/jbm.a.37022
43. Kim J. H., Kim I., Seol Y.-J., Ko I. K., Yoo J. J., Atala A. and Lee S. J. (2020) Neural cell integration into 3d bioprinted skeletal muscle constructs accelerates restoration of muscle function. Nature Communications 11(1):1025. https://doi.org/10.1038/s41467-020-14930-9
44. Sun H., Ma H., Wang L., Liu Y., Hou T., Tang W., Yu Q., An M. and Wen M. (2024) Biomimetic microchannel network with functional endothelium formed by sacrificial electrospun fibers inside 3d gelatin methacryloyl (gelma) hydrogel models. Journal of Zhejiang University-SCIENCE A 25(1):79-96. https://doi.org/10.1631/jzus.A23D0045
45. Luo M., Cheng K., Weng W., Song C., Du P., Shen G., Xu G. and Han G. (2009) Size- and density-controlled synthesis of tio2 nanodots on a substrate by phase-separation-induced self-assembly. Nanotechnology 20(21):215605. https://doi.org/10.1088/0957-4484/20/21/215605